



**AUTHOR(S):**

**TITLE:**

**YEAR:**

**Publisher citation:**

**OpenAIR citation:**

**Publisher copyright statement:**

This is the \_\_\_\_\_ version of an article originally published by \_\_\_\_\_  
in \_\_\_\_\_  
(ISSN \_\_\_\_\_; eISSN \_\_\_\_\_).

**OpenAIR takedown statement:**

Section 6 of the “Repository policy for OpenAIR @ RGU” (available from <http://www.rgu.ac.uk/staff-and-current-students/library/library-policies/repository-policies>) provides guidance on the criteria under which RGU will consider withdrawing material from OpenAIR. If you believe that this item is subject to any of these criteria, or for any other reason should not be held on OpenAIR, then please contact [openair-help@rgu.ac.uk](mailto:openair-help@rgu.ac.uk) with the details of the item and the nature of your complaint.

This publication is distributed under a CC \_\_\_\_\_ license.

\_\_\_\_\_

# Accepted Manuscript

Preparation of 3D spherical Ni/Al LDHs with significantly enhanced electrochemical performance as a superior cathode material for Ni/MH batteries

Yajing Nie, Wei Li, Junqing Pan, Raja Arumugam Senthil, Carlos Fernandez, Abrar Khan, Yanzhi Sun, Jianjun Liu



PII: S0013-4686(18)32015-2

DOI: [10.1016/j.electacta.2018.09.043](https://doi.org/10.1016/j.electacta.2018.09.043)

Reference: EA 32555

To appear in: *Electrochimica Acta*

Received Date: 7 March 2018

Revised Date: 20 August 2018

Accepted Date: 4 September 2018

Please cite this article as: Y. Nie, W. Li, J. Pan, R.A. Senthil, C. Fernandez, A. Khan, Y. Sun, J. Liu, Preparation of 3D spherical Ni/Al LDHs with significantly enhanced electrochemical performance as a superior cathode material for Ni/MH batteries, *Electrochimica Acta* (2018), doi: 10.1016/j.electacta.2018.09.043.

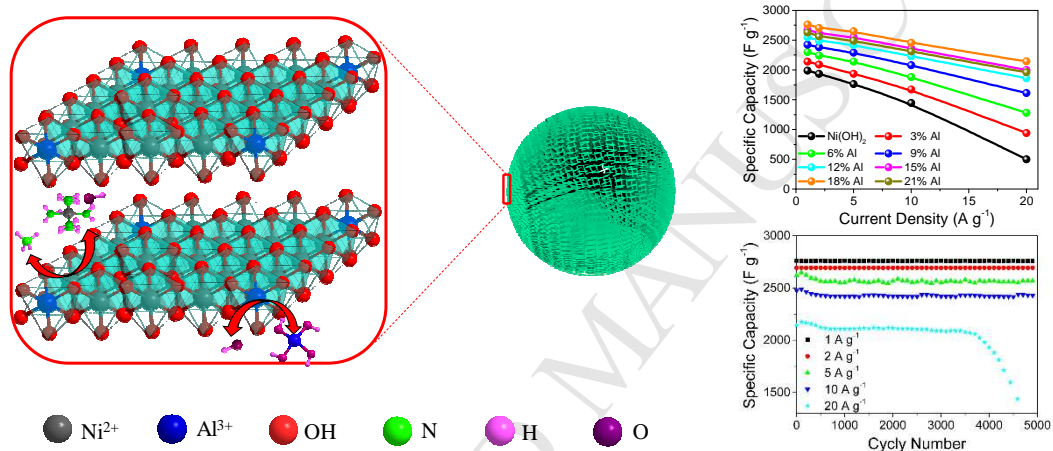
This is a PDF file of an unedited manuscript that has been accepted for publication. As a service to our customers we are providing this early version of the manuscript. The manuscript will undergo copyediting, typesetting, and review of the resulting proof before it is published in its final form. Please note that during the production process errors may be discovered which could affect the content, and all legal disclaimers that apply to the journal pertain.

# Preparation of 3D spherical Ni/Al LDHs with significantly enhanced electrochemical performance as a superior cathode material for Ni/MH batteries

Yajing Nie<sup>a</sup>, Wei Li<sup>b</sup>, Junqing Pan<sup>a,\*</sup>, Raja A. Senthil<sup>a</sup>, Carlos Fernandez<sup>d</sup>, Yanzhi

Sun<sup>c</sup>, Jianjun Liu<sup>a</sup>

Graphical Abstract:



**Preparation of 3D spherical Ni/Al LDHs with significantly enhanced electrochemical performance as a superior cathode material for Ni/MH batteries**

Yajing Nie<sup>a</sup>, Wei Li<sup>b</sup>, Junqing Pan<sup>a,\*1</sup>, Raja Arumugam Senthil<sup>a</sup>, Carlos Fernandez<sup>d</sup>,  
Abrar Khan<sup>a</sup>, Yanzhi Sun<sup>c</sup>, Jianjun Liu<sup>a</sup>

<sup>a</sup> *State Key Laboratory of Chemical Resource Engineering, Beijing University of Chemical Technology, Beijing 100029, China*

<sup>b</sup> *Department of Engineering Technology and Texas Center for Superconductivity, University of Houston, Houston, TX 77204, USA*

<sup>c</sup> *National Fundamental Research Laboratory of New Hazardous Chemicals Assessment and Accident Analysis, Beijing University of Chemical Technology, Beijing 100029, China.*

<sup>d</sup> *School of Pharmacy and Life Sciences, Robert Gordon University, Aberdeen, AB10 7GJ, UK*

\* Corresponding author:

Tel./Fax: +86-10-64448461

E-mails: [jqpan@mail.buct.edu.cn](mailto:jqpan@mail.buct.edu.cn) (J. Pan)

<sup>1</sup> ISE member

**Abstract**

Nickel-based hydroxides with excellent electrochemical performance have been considered as cathode materials for Ni/MH batteries. In this paper, a Ni/Al layered double hydroxides (Ni/Al LDHs) material with three-dimensional (3D) spherical structure is synthesized by a facile stable dual complexation–precipitation method. SEM images show that the obtained Ni/Al LDHs possess 3D spherical structure composed of nanosheets. XRD and CV tests indicate that doping of Al increases the distance between Ni–Al layers, greatly improving the specific capacity of the obtained materials. The electrochemical tests show that the specific capacity of the obtained material with 18% Al is up to 383.4 mAh g<sup>-1</sup> at a current density of 1 A g<sup>-1</sup>. In addition, when the current density is further increased to 10 and 20 A g<sup>-1</sup>, the specific capacity of this material still maintains 345.0 mAh g<sup>-1</sup> and 307.9 mAh g<sup>-1</sup>, respectively, which implies that this cathode material can provide remarkable power densities. Moreover, the material composed of Ni/Al LDHs keeps 97.6% initial capacity after 5,000 cycles at a current density of 10 A g<sup>-1</sup>, showing an excellent cycling stability and durability.

**Keywords:** Ni/Al LDHs; Ni/MH battery; 3D nano structure; cathode material; high charge–discharge speed

## 1. Introduction

In order to reduce the emission of CO<sub>2</sub> by the combustion of fossil fuels, such as coal and gasoline, it is imperative to develop environmentally friendly power sources for the mitigation of climate warming [1–9]. Ni/MH batteries with high power density and good durability are considered as an emerging power source for hybrid electric vehicles. Their extraordinary power capability makes them very promising and suitable for hybrid electric vehicles under heavy load, such as starting and uphill driving. Compared with the existing rechargeable batteries, such as Li-ion batteries, the Ni/MH batteries are limited by their energy density due to low specific capacity of Ni(OH)<sub>2</sub> cathode in practical application [10–12]. Thus they are not suitable to be used as an independent power source for the devices that require a large energy supply. Now, Ni/MH batteries are usually used as an auxiliary power source for hybrid electric vehicles (Prius Hybrid), or as a power source for short-distance buses.

Nickel hydroxide and its derivatives with typical layer structure applied as rechargeable active cathode materials which possess  $\alpha$  and  $\beta$  crystal forms. It is also found that some high-valence metal ions (such as Al<sup>3+</sup>, Co<sup>3+</sup> and Fe<sup>3+</sup>, etc.) replace some of the nickel ions to form new stable layered double hydroxides (LDHs), resulting in maintaining the specific capacity and greatly improving cycle life [13–16]. Zha et al. reported that the specific capacity of Co/Ni LDHs is up to 250.69 – 339.58 mAh g<sup>-1</sup> at a current density of 0.5 A g<sup>-1</sup> [17–22]. Aluminum (Al) is an element of high abundance in Earth crust and can significantly stabilize the structure of Ni/Al LDHs, so it becomes one of the most attractive elements for substitution [19–47].

Many researchers synthesized Ni/Al LDHs with different structures and morphologies by using different methods. Mizuhata reported that the specific capacity of Ni/Al LDHs synthesized by liquid phase deposition was up to about 383.3 mAh g<sup>-1</sup> at 1 A g<sup>-1</sup> and retains 95.1% of the initial value after 300 cycles [23–26]. Li et al. reported that the specific capacity of Ni/Al LDHs by using a self-assembly method is up to 128.5–218.9 mAh g<sup>-1</sup> at 1 A g<sup>-1</sup> [27–29]. Liu and Huang reported a Ni/Al LDHs synthesized by hydrothermal method has a specific capacity of 268.6 and 294.8 mAh g<sup>-1</sup> at 1 A g<sup>-1</sup>, respectively [30, 31]. In addition, the composites of Ni/Al LDHs with porous carbon, nickel foam or graphene have attracted lots of researcher's attentions [32–36]. Yang et al. have reported Ni/Al LDHs/C composite possessing a specific capacity of 127.1–282.5 mAh g<sup>-1</sup> at 1 A g<sup>-1</sup> with a cycling life of 1,000 cycles [32–35]. Wang also reported a Ni/Al LDHs grown on nickel foam possessing a specific capacity of 110.4 mAh g<sup>-1</sup> with a cycle life of 1,000 cycles [36].

According to the Bode cycle, the capacity of an Ni/Al LDHs material can reach an 1.67×X% electron capacity, where X% is the Ni content of the Ni/Al LDHs [39, 42]. Therefore, the theoretical specific capacity of Ni/Al LDHs is 1.67×289×X% mAh g<sup>-1</sup> (483×X% mAh g<sup>-1</sup>) in the working voltage range of 0.1–0.6 V. Obviously, the calculation indicates that the specific capacity of Ni-based LDHs materials still have enough room for improvement. Because the formation K<sub>sp</sub> constant values of Al(OH)<sub>3</sub> and Ni(OH)<sub>2</sub> are pH = 3.7 and 7.2, respectively, there is a large difference between the critical values of the precipitation of Ni<sup>2+</sup> and Al<sup>3+</sup> ions, *i.e.*, a huge amount of Al<sup>3+</sup> ions will firstly induce colloidal precipitate due to the super-saturation degree of the

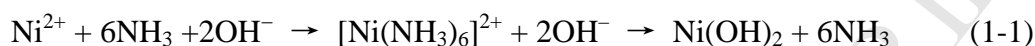
solution before the precipitation of  $\text{Ni}^{2+}$  ions at a high pH value. In these precipitation processes, colloidal precipitate of  $\text{Al}(\text{OH})_3$  with the co-precipitated  $\text{Ni}(\text{OH})_2$  will form disordered Ni/Al co-precipitated microcrystals or colloidal precipitates of  $\text{Al}(\text{OH})_3/\text{Ni}(\text{OH})_2$  composite, resulting in poor electrochemical properties. In addition, these disordered LDHs lack sufficient crystallinity and thus their structures are easily changed during the cycling process, leading to a short cycling life.

Fig. 1 shows the schematic diagram of the formation mechanism of the spherical Ni/Al LDHs with 3D nanostructure and nanosheets synthesized in this study. The obtained spherical particles with an open structure are self-assembled by Ni/Al LDHs nanosheets themselves through a dual complexation–precipitation method. The use of  $\text{Al}(\text{OH})_3$  as a raw material makes the method have a higher atomic economy than other Al sources of traditional methods using Al compounds. For example, when  $\text{Al}_2(\text{SO}_4)_3$  is used, a large amount of  $\text{Na}_2\text{SO}_4$  is produced as a byproduct [40, 44, 45].

In our process,  $\text{Al}(\text{OH})_3$  firstly complexes with NaOH to form  $\text{Al}(\text{OH})_4^-$  ions, which will precipitate again due to the reaction with  $\text{Ni}^{2+}$  ions in a weakly alkaline solution (pH = 11.50). The new process avoids the formation of disordered crystallization of  $\text{Al}(\text{OH})_3$  caused by  $\text{Al}^{3+}$  and  $\text{OH}^-$  through the complex reaction of  $\text{Al}(\text{OH})_3$  and NaOH. The experimental results show that the new structure is not only beneficial to transport of electrons and electrolyte between the nanosheets, but also propitious to alleviation of the structure damage caused by the expansion and contraction between the LDHs layers during charge and discharge processes. So the material with a new open structure consisting of nanosheets and good crystallinity

will support the applications in need of high specific capacitance with excellent durability. In the new process, two complexation precipitation equilibrium reactions take place as follows.

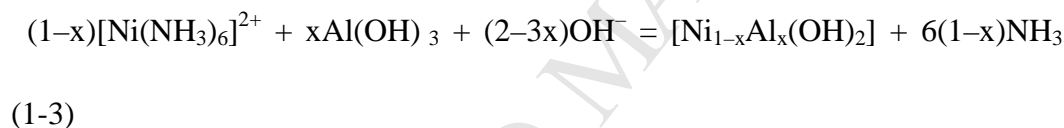
(1) The balance between the precipitation of  $\text{Ni}^{2+}$  and  $\text{OH}^-$  ions is controlled by the complex equilibrium between  $\text{Ni}^{2+}$  and ammonia.



(2) The balance of the precipitation process of  $\text{Al}(\text{OH})_3$  is controlled by the complex equilibrium between  $\text{Al}(\text{OH})_4^-$  and  $\text{OH}^-$ :



The total reaction is:



In order to obtain homogeneous LDHs, the reactions should be carried out in a very stable surrounding with precisely controlled pH and temperature. In the process, the Ni/Al LDHs nanosheets gradually self-assemble via their own spatial orientation structure, meanwhile they slightly dissolve and precipitate again by the balance of the complexation-precipitation of  $\text{Ni}^{2+}$ - $\text{NH}_3$  and  $\text{Al}(\text{OH})_3$ - $\text{OH}^-$ . Finally, Ni/Al LDHs spherical particles with open structure of nanosheets are formed. Electrochemical tests show that the material provides a larger specific capacity and longer cycling life than the conventional Ni/Al LDHs reported in the literatures.

## 2 Experimental Section

## 2.1 Synthesis of Ni/Al LDHs

$\text{NH}_3\cdot\text{H}_2\text{O}$ , NaOH, and  $\text{NiSO}_4$  of AR grade were purchased from Beijing Jingxi Refined Chemicals Regent. 30 mL  $1.2 \text{ mol L}^{-1}$   $\text{NH}_3\cdot\text{H}_2\text{O}$  solution was added to a 100 mL three-neck round-bottom glass flask and heated up to  $50 \text{ }^\circ\text{C}$  for reaction by a super water bath (DF-101S, Beijing Sunny Science Instrument). The solution was stirred constantly at a stirring speed of 150 rpm. Then 8 mL  $\text{NiSO}_4$  solution ( $1.2 \text{ mol L}^{-1}$ ), marked as solution A, and 8 mL  $\text{Al}(\text{OH})_3\text{-NaOH-NH}_3$  solution ( $0.25 \text{ mol L}^{-1}$  of  $\text{Al}(\text{OH})_3$ ,  $2.4 \text{ mol L}^{-1}$  of NaOH,  $2.4 \text{ mol L}^{-1}$  of  $\text{NH}_3\cdot\text{H}_2\text{O}$ ) containing  $3 \text{ mol L}^{-1}$  of DPE-3 (crystallization additive, Nanjing Eurotronic Chemical), marked as solution B, were simultaneously pumped into the reactor at a rate of  $0.25 \text{ mL min}^{-1}$  by two peristaltic pumps separately (DH100B, Baoding Longer Pumps). The pH of the reaction mother solution was monitored by a HANNA pH meter (pH211) and controlled at  $11.5 \pm 0.03$  by accurately adjusting the flow rate of solution A around  $0.25 \pm 0.01 \text{ mL min}^{-1}$ . The reaction mixture was stirred continuously for 16 h at  $50 \text{ }^\circ\text{C}$  as an aging process after finishing the pumping of the above solutions. The product was filtrated and washed with  $50 \text{ }^\circ\text{C}$  deionized (DI) water till the washing liquid presents neutral, and finally dried in a vacuum oven at  $60 \text{ }^\circ\text{C}$  for 3 h. For optimization and comparison tests, other samples with different contents of Al and without Al were also prepared using the same process.

## 2.2 Morphology and Structure Characterizations

The morphology of the synthesized samples was examined using a scanning electron microscope equipped with energy dispersive spectrometer (SEM/EDX, Zeiss

SUPRA 55) at an accelerating voltage of 20 kV. The crystalline structure was characterized by X-ray diffraction (XRD) on a Bruker D8 Advance X-Ray Diffractometer using a Cu K $\alpha$  source at a scanning rate of 10° min<sup>-1</sup> and a scanning angle (2 $\theta$ ) range from 5° to 90°. Spectrograms of X-ray photoelectron spectroscopy (XPS) were collected on a PHI 5000C ESCA ESCALAB 250 instrument with Al K $\alpha$  radiation. The binding energies were determined with adventitious carbon (C1s at 284.6 eV) as the reference. Transmission electron microscope (TEM) images were obtained on a Philips CM200FEG Field Emission Microscope.

### 2.3 Electrochemical Measurements

A mixture of 200 mg sample, 60 mg expanded graphite (99.9%, Qingdao Laixi Fine Graphite), 50 mg PTFE (60 wt.%, Guangzhou Songbai Chemicals), and 100  $\mu$ L DI water was mixed and ground in an agate mortar for 30 min. The obtained paste was roll-pressed into a 50  $\mu$ m thick film as an electrode film. An electrode film sample with a size of 10 mm  $\times$  10 mm was then pressed on a same size nickel foam film (density: 550  $\pm$  30 g m<sup>-2</sup>, pores per inch: 100  $\pm$  30, thickness: 1.8  $\pm$  0.1 mm, purchased from Changsha Liyuan New Materials) by using a powder pressing machine (YP-15A, Shanghai Jingsheng Instrument) at 10 MPa for 3 min to form a cathode sample.

Electrochemical measurements were carried out in 1.0 mol L<sup>-1</sup> KOH in a three-electrode system cell at room temperature (around 298 K). An above prepared cathode was used as the work electrode. A 10 mm  $\times$  10 mm nickel plate and an HgO/Hg electrode were used as auxiliary electrode and reference electrode,

respectively. Charging/discharging (scan range: 0.1–0.6 V, current density: 1–20 A g<sup>-1</sup>) experiments were carried on a LAND–CT2001A battery test system. The experiments of cyclic voltammetry (CV, scan range: –0.25–1.05 V, scan rate: 1–50 mV s<sup>-1</sup>) and electrochemical impedance spectroscopy (EIS, frequency range: 0.01–10<sup>5</sup> Hz, AC potential: 5 mV) were carried out on an electrochemistry workstation (CHI 760D, Shanghai CH Instrument).

### 3. Results and Discussion

Fig. 2a-h show the morphology and mapping images of the obtained Ni/Al LDHs samples with different contents of Al. It can be seen that all the samples present a spherical shape with stack of nanosheets. The Ni/Al LDHs nanosheets become thinner as the Al content gradually increases in the range of 0 to 18%. It is beneficial to increasing specific surface area of the Ni/Al LDHs nanosheets, which increases the contact area of the sample particles and the electrolyte as well as shortens the proton and electron migration paths, resulting in the increase of charge and discharge speeds. When the Al content reaches 21%, Ni/Al LDHs presents agglomeration phenomenon between the nanosheets. The BET results in Table S1 also show that the highest surface area is observed when the Al content is 18%, so the optimal Al content should be controlled below 21%. The EDX mapping images of the samples with different Al contents verify the gradual increase of Al contents in the samples as expected.

Fig. 2i shows the XRD patterns of the Ni/Al LDHs samples with different Al contents. When the Al content is 0, the peaks of the sample appear at  $2\theta = 19.26^\circ$ ,  $33.14^\circ$ ,  $38.42^\circ$ ,  $51.96^\circ$ ,  $59.04^\circ$  and  $62.78^\circ$ , corresponding to (001), (100), (101), (102),

(110) and (111) peaks of the standard card of  $\beta$ -Ni(OH)<sub>2</sub> (JCPDS14-0117), respectively. The results demonstrate that the lattice parameters of the Ni/Al LDHs containing 0% Al are  $a = b = 0.3126$  nm and  $c = 0.4638$  nm, which are very close to the lattice parameters of pure  $\beta$ -Ni(OH)<sub>2</sub> ( $a = b = 0.3126$  nm,  $c = 0.4605$  nm). This indicates that the Ni/Al LDHs sample (0% Al) has the same crystal structure as  $\beta$ -Ni(OH)<sub>2</sub> (phase  $\beta$ ), *i.e.*, a typical structure of layered hexagonal crystal brucite. When Al content continues to increase 6%, it is observed that two peaks occur on the XRD pattern at  $2\theta = 11.84^\circ$  and  $23.56^\circ$ , corresponding to the characteristic diffraction peaks of (003) and (006) facets of  $\alpha$ -Ni(OH)<sub>2</sub>, respectively, indicating that the crystal structure of the Ni/Al LDHs begins to convert into  $\alpha$ -Ni(OH)<sub>2</sub> (phase  $\alpha$ ). When Al content further increases to or exceeds 12%, only pure phase of  $\alpha$ -Ni(OH)<sub>2</sub> is observed. Therefore, Ni/Al LDHs samples with hybrid of phase  $\alpha$  and  $\beta$  can be obtained by controlling the Al content between 3% and 12%.

As seen from Fig. 2i, a typical sample with 15% or 18% Al shows two peaks at  $2\theta = 11.84^\circ$  and  $23.56^\circ$ , corresponding to the diffraction peaks (0 0 3) and (0 0 6) of  $\alpha$ -Ni(OH)<sub>2</sub> (JCPDS38-0715), respectively. In the  $2\theta$  region of  $33\sim 39^\circ$ , two small diffraction peaks appear as the characteristic peaks of  $\alpha$ -Ni(OH)<sub>2</sub> with vortex lamellar structure.

Table S2 presents the lattice parameters calculated from the XRD spectra of Fig. 2 by Scherrer formula, where the value of parameter  $a$  depends on the distance between the metal atoms and the oxygen atoms, and value  $c$  depends on the distance between the NiO<sub>2</sub> layers. It is observed that the value of  $a$  gradually decreases while

the value of  $c$  gradually increases as the Al content rises. The Al–O bond length (0.194 nm) is shorter than the Ni–O bond length (0.209 nm), so a part of the Ni atoms is replaced by Al atoms, leading to a tendency to gradually decrease of the value of  $a$ . At the same time, due to the difference of the charge number between  $\text{Al}^{3+}$  and  $\text{Ni}^{2+}$ , the increase in Al content causes an excess positive charge on the  $\text{NiO}_2$  layers, which causes an insertion of a part of anions and water molecules into the interlayers, resulting in  $\bar{c}$ -axis expansion. The increase in spacing between LDHs layers is beneficial to accelerating the diffusion of protons between layers and improving electrochemical performance of the sample during charge and discharge processes. However, excessive  $\text{Al}^{3+}$  ions can cause more anions to clog the LDHs interlayers, which will block the exchange of ions between the layers and electrolyte and in turn cause a decrease in electrochemical performance of the sample. Therefore, the Al content should not be too high in the Ni/Al LDHs samples for optimal performance.

Fig. 3a shows the CV curves of the samples with an Al content from 0 to 21% at a scan rate of  $10 \text{ mV s}^{-1}$ . It can be seen that when the Al content increases from 0 to 18%, the redox peak current of the sample electrode rises. The sample with 18% Al provides the maximum redox peak current, indicating that it has the best electrochemical performance. When the Al content further increases to 21%, the redox peak current decreases, suggesting that extra high content of Al causes the decrease in electrochemical performance, which is consistent with the results from previous XRD analysis.

Fig. 3b shows the charge and discharge specific capacities of the samples with

different Al contents during the above CV tests, and the calculation formula of the specific capacity is as follows:

$$Q = \frac{1}{ms} \int_{V_i}^{V_f} I(V) dV \quad (1-4)$$

where  $m$  is the mass of active electrode material,  $s$  is the potential scan rate,  $V_f$  and  $V_i$  are the integration limits of a voltametric curve, and  $I(V)$  denotes the response current density.

As seen from Fig. 3b, with increasing Al content, the specific capacity of the samples presents a gradual increase before the point of 18% Al, followed by a gradual decrease thereafter. When the Al content is 18%, the specific capacity reaches the maximum value ( $336.67 \text{ mAh g}^{-1}$ ), suggesting that the optimum doping amount of Al is 18%.

Fig. 3c shows the charge–discharge curves of the samples with Al contents from 0 to 21% at  $2 \text{ A g}^{-1}$ . It can be seen that the curves appear relatively flat, indicating the Ni/Al LDHs have typical oxidation peak and reduction peak during the charge and discharge processes. The specific capacity of the samples can be calculated in according to the following formula (5):

$$Q = i \times t / m \quad (1-5)$$

where  $i$ ,  $t$ , and  $m$  correspond to the discharge current, discharge time for charge/discharge, and mass of active electrode material, respectively.

The calculated specific capacity of Ni/Al LDHs with Al contents of 0%, 3%, 6%, 9%, 12%, 15%, 18% and 21% at  $2 \text{ A g}^{-1}$  are 268.8, 290.2, 311.6, 330.6, 345.7, 363.1, 375.6 and  $355.9 \text{ mAh g}^{-1}$ , respectively. The charge and discharge experiments show

that the specific capacity of Ni/Al LDHs rises with increasing Al content from 0 to 18% and decreases as Al content exceeds 18%. Therefore, the optimal Al content of Ni/Al LDHs with the maximum specific capacity is 18%.

Fig. 3d shows the specific capacity curves of the samples at different current densities. As Al content increases, the discharge capacity increases first, and the highest specific capacity of the samples is achieved when the Al content reaches 18%. The results also indicate that the sample with 18% Al offers higher rate performance than other samples with different Al contents under heavy load. When the current density is 1, 2, 5, 10 and 20 A g<sup>-1</sup>, the sample with 18% Al content provides specific capacity of 383.4, 375.6, 369.1, 345.0 and 307.9 mAh g<sup>-1</sup>, respectively, which are much higher than the corresponding figures of those LDHs materials reported in the literature [12–15, 30, 33–36].

Fig. S1a shows the Nyquist plots from AC impedance experiments of the Ni/Al LDHs samples with Al content from 0 to 18%. It can be seen that as Al content increases, the semi-circular arcs in the low frequency region gradually reduce, suggesting that the doping of Al is beneficial to reducing the polarization impedance of the electrochemical reaction. When the Al content goes up to 21%, the semi-circular arcs increase instead, implying that the best Al content is 18%.

Fig. S1b shows the polarization curves from Tafel tests of the sample electrodes and the exchange current densities obtained from the polarization curves are listed in Table S3. The results show that the exchange current densities rise with increasing Al content from 0 to 18%. The exchange current densities of the samples with Al

contents from 0 to 18% monotonically increase in the range of  $16.85 \text{ mA cm}^{-2}$  to  $21.07 \text{ mA cm}^{-2}$ . The results are well consistent with the results of the previous AC impedance tests, indicating that the sample with 18% Al has the highest electrochemical activity.

According to the former XRD and electrochemical test results from in Fig. 2 and 3, respectively, Fig. 4a shows the change in the average of parameter  $c$  ( $\bar{c}$ ) with increasing Al content. It is found that the distance of  $c$  rapidly rises as Al content increases in the range of 0–15%, and it becomes stable when Al content increases from 15% to 21%. As calculated from Fig. S1b, the increase in the distance of  $c$  ( $\bar{c}$ ) will weaken the interlayer bonding force of LDHs layers and significantly contribute to the increase in exchange current density and electrochemical performance of Ni/Al LDHs (Fig. 4a). This force can be considered as the positive effect for the increase in electrochemical performance (blue line in Fig.4b, denoting Positive forces 1). However, the excessive amounts of  $\text{Al}^{3+}$  replacing  $\text{Ni}^{2+}$  in LDHs lattice and the excessively positive charge will attract other anions or electronegative molecules from electrolyte around the Ni/Al LDHs, such as  $\text{OH}^-$  or  $\text{H}_2\text{O}$ , thus affecting the diffusion and exchange of proton and electrolyte (red line 1 in Fig.4b, standing for Negative forces 1).

In addition, when the Al content exceeds 18%, extra longer distance between the layers is easy for the anions to insert, which will also block the discharge and charge processes of Ni/Al LDHs (red line 2 in Fig.4b, denoting Negative forces 2). Fig. 4c-d display the possible mechanism schematic of the doping of different amounts of Al

and its comprehensive results of the above three forces (Positive forces 1 + Negative forces 1 + Negative forces 2) on the structure and electrochemical properties of the Ni/Al LDHs samples. Obviously, the 18% Al-doped Ni/Al LDHs sample shows the best electrochemical performance.

Fig. 5a shows the XRD patterns of the 18% Al-doped Ni/Al LDHs sample under different charge and discharge states. It can be seen that the initial state of the sample has a crystal structure of  $\alpha$ -Ni(OH)<sub>2</sub> (JCPDS38-0715). The metallic Ni peaks shown in the pattern are derived from the nickel foam in the electrode. As the charge process proceeds, it is found that characteristic diffraction peaks of (003) and (006) facets are weakened and the characteristic diffraction peak of (006) facet of  $\gamma$ -NiOOH at  $2\theta = 26.2^\circ$  appears at half charged state. When the sample is fully charged, the characteristic diffraction peaks of  $\alpha$ -Ni(OH)<sub>2</sub> disappear and the XRD pattern shows diffraction peaks at  $2\theta = 26.2^\circ, 44.4^\circ, 52.3^\circ$  and  $77.8^\circ$ , corresponding to the characteristic diffraction peaks of  $\gamma$ -NiOOH, meaning that the Ni/Al LDHs is substantially oxidized into  $\gamma$ -NiOOH after fully charged. It can also be found that no other diffraction peaks appear during the charge process, suggesting that the  $\alpha/\gamma$  phase cycle does not undergo a mesophase. Similarly, all the  $\gamma$ -NiOOH is converted into  $\alpha$ -Ni(OH)<sub>2</sub> after fully charged, showing that the charge and discharge processes of Ni/Al LDHs are stably reversible in the  $\alpha$  and  $\gamma$  phase cycle. The Ni/Al LDHs provides higher specific capacity and longer lifetime because the electron transfer number of  $\alpha$ -Ni(OH)<sub>2</sub>/ $\gamma$ -NiOOH can achieve up to 1.67 while that of the traditional  $\beta$ -Ni(OH)<sub>2</sub>/ $\beta$ -NiOOH process is 1.

We also analyzed the change in valence of the Ni in 18% Al-doped Ni/Al LDHs during charge and discharge processes. As seen from the XPS spectra in Fig. 5b, the enlarged initial state shows Ni 2p XPS spectrum with two major peaks of Ni 2p<sub>3/2</sub> (856.5 eV) and Ni 2p<sub>1/2</sub> (874.2 eV) as well as their corresponding satellite peaks. When the electrode begins to charge to the half charged state, the Ni 2p<sub>3/2</sub> peak starts to be split into two peaks, namely, Ni peak of  $\alpha$ -Ni(OH)<sub>2</sub> at 856.7 eV and Ni peak of  $\gamma$ -NiOOH at 858.8 eV. And Ni 2p<sub>1/2</sub> peak starts to be split into the Ni peak of  $\alpha$ -Ni(OH)<sub>2</sub> at 874.4 eV and Ni peak of  $\gamma$ -NiOOH at 877.7 eV.

When the electrode is fully charged, the two split peaks of Ni 2p<sub>3/2</sub> and Ni 2p<sub>1/2</sub> are completely transformed into the  $\gamma$ -NiOOH peaks. For example, the Ni 2p<sub>3/2</sub> (856.5 eV) peak of  $\alpha$ -Ni(OH)<sub>2</sub> is fully converted into the Ni 2p<sub>3/2</sub> (858.9 eV) peak of  $\gamma$ -NiOOH and the Ni 2p<sub>1/2</sub> (874.2 eV) peak of  $\alpha$ -Ni(OH)<sub>2</sub> is also completely converted into the Ni 2p<sub>1/2</sub> (877.6 eV) peak of  $\gamma$ -NiOOH. Similarly, it is observed that the Ni 2p<sub>1/2</sub> (877.6 eV) and Ni 2p<sub>3/2</sub> (858.9 eV) peaks of  $\gamma$ -NiOOH are completely converted into Ni 2p<sub>1/2</sub> (873.2.3 eV) and Ni 2p<sub>3/2</sub> (856.3 eV) peaks of  $\alpha$ -Ni(OH)<sub>2</sub>, respectively after the electrode is completely discharged.

Fig. 5c and e show the TEM images of 18% Al-doped sample (Ni/Al LDHs) before charge and discharge with different magnifications. It can be seen from Fig. 5c that the shape of the Ni/Al LDHs sample is approximately spherical, which is consistent with the SEM images in Fig. 2. In addition, the lattice fringes in Fig. 5d indicate a single lattice spacing of 0.397 nm corresponding to the (006) facet of  $\alpha$ -Ni(OH)<sub>2</sub>. Fig. 5d and f are the TEM images with different magnifications for 18%

Al-doped sample (Ni/Al LDHs) after 5,000 cycles. Comparing Fig. 5e with f, the HR-TEM images of the two samples show that the structure of the Ni/Al LDHs keeps stable during charge and discharge processes.

Fig. 6a shows the CV curves of the Ni/Al LDHs sample with 18% Al at different scan rates. The response current density of the CV curves increases with scanning rate, which indicates that the sample has good electrochemical performance. The charge and discharge specific capacity of the CV processes are calculated and the results are plotted in Fig. 6b. It can be seen that the specific capacity of the sample can reach 375.2 mAh g<sup>-1</sup> at 1 mV s<sup>-1</sup>. When the scan rate increases to 50 mV s<sup>-1</sup>, the specific capacity of the sample still retains 190.7 mAh g<sup>-1</sup>, indicating that the sample has excellent quick charge and discharge performance.

Fig. 6c shows the durability of the sample with 18% Al under different current densities from 1 to 20 A g<sup>-1</sup>. The results show that the specific capacities of the electrodes are very stable. When the charge–discharge current density increases from 1, 2, 5 to 10 A g<sup>-1</sup>, only about 0.2%, 0.3%, 1.2% and 2.4% of initial capacity decline are observed after 5,000 cycles, respectively, indicating the obtained samples have excellent durability under high rate performance. When the current density further increases to 20 A g<sup>-1</sup>, the discharge specific capacity remains stable during the first 3,850 cycles, still providing 297.7 mAh g<sup>-1</sup>. Electrochemical tests show that the sample with spherical structure and open nanosheets not only benefits the transport of electrons and electrolyte, but also helps LDHs lattice and layers reduce the stress of expansion and contraction during the charge and discharge processes. Therefore, it

can provide higher specific capacity with excellent durability.

Fig. 6d shows the comparison of the specific capacity of the Ni/Al LDHs sample containing 18% Al with the nickel hydroxide materials reported in the literature at different current densities. It can be seen that the Ni/Al LDHs sample has superior electrochemical properties to the reported materials in terms of capacity and power performance.

#### 4. Conclusions

In this paper, a kind of Ni/Al LDHs materials are synthesized by a dual complexation-precipitation method at precisely conditions of controlled pH and temperature. The XRD results show that the Ni/Al LDHs sample with 18% Al has the best structure for charge and discharge processes. The CV and charge-discharge experiments also show that the sample with 18% Al has the optimal electrochemical performance with a high specific capacity of  $383.4 \text{ mAh g}^{-1}$  at  $1 \text{ A g}^{-1}$ . The XRD and XPS analyses of the samples at various charge and discharge states indicate that the transformation between  $\alpha\text{-Ni(OH)}_2$  and  $\gamma\text{-NiOOH}$  of the Ni/Al LDHs is stable and reversible during charge and discharge processes. Beneficial from the optimized layered structure with well-regulated nanosheets, the Ni/Al LDHs cathode offers superior specific capacity, rate performance, and cycle durability than the LDHs materials reported in the literature.

#### Acknowledgements

This work was supported by National Natural Science Foundation of China (21676022 & 21706004), and the Fundamental Research Funds for the Central Universities (BHYC1701A & JD1701).

ACCEPTED MANUSCRIPT

**Reference**

- [1] X. Xu, M. Wang, Y. Liu, Y. Li, T. Lu, L. Pan, In situ construction of carbon nanotubes/nitrogen-doped carbon polyhedral hybrids for supercapacitors, *Energy Storage Materials*, 5 (2016) 132–138.
- [2] S. Osman, R. A. Senthil, J. Pan, W. Li, Highly activated porous carbon with 3D microspherical structure and hierarchical pores as greatly enhanced cathode material for high performance supercapacitors, *Journal of Power Sources*, 391 (2018) 162–169.
- [3] Y. Fang, B. Luo, Y. Jia, X. Li, B. Wang, Q. Song, F. Kang, L. Zhi, Renewing Functionalized Graphene as Electrodes for High-Performance Supercapacitors, *Advanced Materials*, 24 (2012) 6348–6355.
- [4] D. Zhou, Z. Cai, X. Lei, W. Tian, Y. Bi, Y. Jia, N. Han, T. Gao, Q. Zhang, Y. Kuang, J. Pan, X. Sun, X. Duan, NiCoFe-Layered Double Hydroxides/N-Doped Graphene Oxide Array Colloid Composite as an Efficient Bifunctional Catalyst for Oxygen Electrocatalytic Reactions, *Advanced Energy Materials*, 1701905 (2017), 1–7.
- [5] T. Wang, M. Yang, J. Pan, A New Single Flow Zinc-Nickel Hybrid Battery Using a Ni(OH)<sub>2</sub>-O<sub>2</sub> Composite cathode, *International Journal Electrochemical Science*, 12 (2017) 6022 – 6030
- [6] C. Choi, J. A. Lee, A Y. Choi, Y. T. Kim, X. Lepró, M. D. Lima, R. H. Baughman, and S. J. Kim, Flexible Supercapacitor Made of Carbon Nanotube Yarn with Internal Pores, *Advanced Materials*, 26 (2014) 2059–2065.
- [7] X. Fan, C. Yu, J. Yang, Z. Ling, C. Hu, M. Zhang, and J. Qiu, A Layered-Nanospace-Confinement Strategy for the Synthesis of Two-Dimensional Porous Carbon Nanosheets for High-Rate Performance Supercapacitors, *Advanced Energy Materials*, 5 (2015) 1401761–1401767.
- [8] Y. Pan, Y. Zhao, S. Mu, Y. Wang, C. Jiang, Q. Liu, Q. Fang, M. Xue and S. Qiu, Cation exchanged MOF-derived nitrogen-doped porous carbons for CO<sub>2</sub> capture and supercapacitor electrode materials, *Journal of Materials Chemistry A*, 5

- (2017) 9544–9552.
- [9] K. Wang, Y. Cao, X. Wang, Q. Fan, W. Gibbons, T. Johnson, B. Luo, Z. Gu, Pyrolytic cyanobacteria derived activated carbon as high performance electrode in symmetric supercapacitor, *Energy*, 94 (2016) 666–671.
- [10] T. Wang, J. Pan, K. G. Achille, Y. Sun, A green dual complexation precipitation synthesis of hierarchical  $\alpha$ -Ni(OH)<sub>2</sub> microspheres and their electrochemical performance, *International Journal of Hydrogen Energy*, 42 (2017) 19139–19147.
- [11] J. Pan, M. Yang, Y. Sun, T. Ma, X. Yue, W. Li, X. Sun, Totally atom-economical synthesis of nano/micro structured nickel hydroxide realized by an Ni–O<sub>2</sub> fuel cell, *Green Chemistry*, 17 (2015) 1446–1452.
- [12] X. Yue, J. Pan, Y. Sun, Z. Wang, Synthesis and Electrochemical Properties of Nano–Micro Spherical  $\beta$ -Ni(OH)<sub>2</sub> with Super High Charge–Discharge Speed, *Industrial Engineering Chemistry Research*, 51(2012) 8358–8365
- [13] X. Yang, J. Pan, Y. Nie, Y. Sun, P. Wan, A facile and scalable complexation-precipitation method of iron doped nickel hydroxide nanosheets as a superior oxygen evolution catalyst, *International Journal of Hydrogen Energy*, 42 (2017) 26575–26585.
- [14] W. Liu, C. Ju, D. Jiang, L. Xu, H. Mao, K. Wang, Ionic liquid-assisted grown of beta-nickel hydroxide nanowires on reduced graphene oxide for high-performance supercapacitors, *Electrochimica Acta*, 143 (2014) 135–142.
- [15] M. Xie, S. Duan, Y. Shen, K. Fang, Y. Wang, M. Lin, X. Guo, In–Situ–Grown Mg(OH)<sub>2</sub>–Derived Hybrid  $\alpha$ -Ni(OH)<sub>2</sub> for Highly Stable Supercapacitor, *ACS Energy Letter*, 1 (2016) 814–819.
- [16] H. Du, L. Jiao, K. Cao, Y. Wang, and H. Yuan, Polyol–Mediated Synthesis of Mesoporous  $\alpha$ -Ni(OH)<sub>2</sub> with Enhanced Supercapacitance. *ACS Applied Materials & Interfaces*, 5 (2013) 6643–6648.
- [17] D. Zha, H. Sun, Y. Fu, X. Ouyang, X. Wang, Acetate anion–intercalated nickel–cobalt layered double hydroxide nanosheets supported on Ni foam for high–

- performance supercapacitors with excellent long-term cycling stability, *Electrochimica Acta*, 236 (2017) 18–27;
- [18] T. Yan, R. Li, T. Yang, Z. Li, Nickel/cobalt layered double hydroxide hollow microspheres with hydrangea-like morphology for high-performance supercapacitors, *Electrochimica Acta*, 152 (2015) 530–537.
- [19] Y. Cheng, H. Zhang, C. V. Varanasi and J. Liu, Improving the performance of cobalt–nickel hydroxide–based self–supporting electrodes for supercapacitors using accumulative approaches, *Energy & Environmental Science*, 6 (2013) 3314–3321.
- [20] X. Wang, A. Sumboja, M. Lin, J. Yan and P. S. Lee, Enhancing electrochemical reaction sites in nickel–cobalt layered double hydroxides on zinc tin oxide nanowires: a hybrid material for an asymmetric supercapacitor device, *Nanoscale*, 4 (2012) 7266–7272;
- [21] N. T. H. Trang, H. V. Ngoc, N. Lingappan, D. J. Kang, A comparative study of supercapacitive performances of nickel cobalt layered double hydroxides coated on ZnO nanostructured arrays on textile fibre as electrodes for wearable energy storage devices, *Nanoscale*, 6 (2014) 2434–2439.
- [22] K. P. Annamalai, L. Liu, Y. Tao, Highly Nanoporous Nickel Cobaltite Hexagonal Nanostructure–Graphene Composites for the Next Generation Energy Storage/Conversion Devices, *Advanced Materials*, 1700219 (2017) 1–8.
- [23] H. Maki, M. Takigawa, M. Mizuhata, Nickel–Aluminum Layered Double Hydroxide Coating on the Surface of Conductive Substrates by Liquid Phase Deposition, *ACS Applied Materials & Interfaces*, 31 (2015) 17188–17198.
- [24] A. B. Béléké, E. Higuchi, H. Inoue, M. Mizuhata, Effects of the composition on the properties of nickel–aluminum layered double hydroxide carbon (Ni–Al LDH/C) composite fabricated by liquid phase deposition (LPD) , *Journal of Power Sources*, 225 (2013) 215–220.
- [25] A. B. Béléké, E. Higuchi, H. Inoue, M. Mizuhata, Durability of nickel–metal hydride (Ni–MH) battery cathode using nickel–aluminum layered double

- hydroxide/carbon (Ni–Al LDH/C) composite, *Journal of Power Sources*, 247 (2014) 572–578.
- [26] A. B. Béléké, M. Mizuhata, Electrochemical properties of nickel–aluminum layered double hydroxide carbon composite fabricated by liquid phase deposition, *Journal of Power Sources*, 195 (2010) 7669–7676.
- [27] H. Li, Z. Chen, Y. Wang, J. Zhang, X. Yan, Controlled synthesis and enhanced electrochemical performance of self–assembled rosette–type Ni–Al layered double hydroxide, *Electrochimica Acta*, 210 (2016) 15–22.
- [28] M. Du, X. Yin, C. Tang, T. J. Huang, H. Gong, Takovite–derived 2–D Ni Al double hydroxide monolayer and graphene hybrid electrodes for electrochemical energy storage applications with high volumetric capacitance, *Electrochimica Acta*, 190 (2016) 521–530.
- [29] X. Ge, C. Gu, Z. Yin, X. Wang, J. Tu, J. Li, Periodic stacking of 2D charged sheets: Self–assembled superlattice of Ni–Al layered double hydroxide (LDH) and reduced graphene oxide, *Nano Energy*, 20 (2016) 185–193.
- [30] H. Liu, T. Yu, D. Su, Z. Tang, J. Zhang, Y. Liu, A. Yuan, Q. Kong, Ultrathin Ni–Al layered double hydroxide nanosheets with enhanced supercapacitor performance, *Ceramics International*, 43 (2017) 14395–14400.
- [31] J. Huang, T. Lei, X. Wei, X. Liu, T. Liu, D. Cao, J. Yin, G. Wang, Effect of Al–doped  $\beta$ –Ni(OH)<sub>2</sub> nanosheets on electrochemical behaviors for high performance supercapacitor application, *Journal of Power Sources*, 232 (2013) 370–375.
- [32] W. Yang, Z. Gao, J. Wang, J. Ma, M. Zhang, L. Liu, Solvothermal One–step Synthesis of Ni–Al Layered Double Hydroxides/Carbon Nanotube/Reduced Graphene Oxide Sheet Ternary Nanocomposite with Ultrahigh Capacitance for Supercapacitors, *ACS Applied Materials & Interfaces*, 12 (2013) 5443–5454.
- [33] Y. Wang, Z. Chen, H. Li, J. Zhang, X. Yan, K. Jiang, D. Engelsen, L. Ni, D. Xiang, The synthesis and electrochemical performance of core–shell structured Ni–Al layered double hydroxide carbon nanotubes composites, *Electrochimica Acta*, 222 (2016) 185–193.

- [34] Y. Wimalasiri, R. Fan., X. S. Zhao, L. Zou, Assembly of Ni–Al layered double hydroxide and graphene electrodes for supercapacitors, *Electrochimica Acta*, 134 (2014) 127–135.
- [35] F. He, Z. Hu, K. Liu, S. Zhang, H. Liu, S. Sang, In situ fabrication of nickel aluminum–layered double hydroxide nanosheets/hollow carbon nanofibers composite as a novel electrode material for supercapacitors, *Journal of Power Sources*, 267 (2014) 188–196.
- [36] B. Wang, Q. Liu, Z. Qian, X. Zhang, J. Wang, Z. Li, H. Yan, Z. Gao, F. Zhao, L. Liu, Two steps in situ structure fabrication of Ni–Al layered double hydroxide on Ni foam and its electrochemical performance for supercapacitors, *Journal of Power Sources*, 246 (2014) 747–753.
- [37] Z. Yin, J. Wu, Z. Yang, Amperometric sensors based on Ni/Al and Co/Al layered double hydroxides modified electrode and their application for hydrogen peroxide detection, *Biosensors and Bioelectronics*, 26 (2011) 1970–1974.
- [38] V. Mas, M. L. Dieuzeide, M. Jobbágy, G. Baronetti, N. Amadeo, M. Laborde, Ni(II)–Al(III) layered double hydroxide as catalyst precursor for ethanol steam reforming: Activation treatments and kinetic studies, *Catalysis Today*, 133–135 (2008) 319–323.
- [39] J. Hu, G. Lei, Z. Lu, K. Liu, S. Sang, H. Liu, Alternating Assembly of Ni–Al Layered Double Hydroxide and Graphene for High–Rate Alkaline Battery Cathode, *Chemical Communications*, 51 (2015) 9983–9986.
- [40] H. Chen, J. M. Wang, T. Pan, H. M. Xiao, J. Q. Zhang, C. N. Cao, Effects of coprecipitated zinc on the structure and electrochemical performance of Ni/Al–layered double hydroxide, *International Journal of Hydrogen Energy*, 27 (2002) 489–496.
- [41] J. Li, E. Shangguan, M. Nie, Q. Jin, K. Zhao, Z. Chang, X–Z. Yuan, H. Wang, Enhanced electrochemical performance of high–density Al–substituted  $\alpha$ –nickel hydroxide by a novel anion exchange method using NaCl solution, *International Journal of Hydrogen Energy*, 40 (2015) 1852–1858.

- [42] O. Cairon, E. Dumitriu, C. Guimon, Acido–basicity of Mg–Ni–Al Mixed Oxides from LDH Precursors A FTIR and XPS Study, *Journal of the American Chemical Society*, 111 (2007) 8015–8023.
- [43] J–F. Yang, Z–T. Zhou, Use of spray technique to prepare Ni Al–layered double hydroxides, *Journal of Alloys and Compounds*, 473 (2009) 458–461.
- [44] C. Miao, Y. Zhu, L. Huang, T. Zhao, The relationship between structural stability and electrochemical performance of multi–element doped alpha nickel hydroxide, *Journal of Power Sources*, 274 (2015) 186–193.
- [45] E. Shanguan, J. Li, D. Guo, L. Guo, M. Nie, Z. Chang, X–Z. Yuan, H. Wang, A comparative study of structural and electrochemical properties of high–density aluminum substituted  $\alpha$ –nickel hydroxide containing different interlayer anions, *Journal of Power Sources*, 282 (2015) 158–168.
- [46] J. Li, E. Shanguan, D. Guo, M. Tian, Y. Wang, Q. Li, Z. Chang, Xiao–Zi Yuan, H. Wang, Synthesis, characterization and electrochemical performance of high–density aluminum substituted  $\alpha$ –nickel hydroxide cathode material for nickel–based rechargeable batteries, *Journal of Power Sources*, 270 (2014) 121–130.
- [47] J. Yao, Y. Li, Y. Li, Y. Zhu, H. Wang, Enhanced cycling performance of Al–substituted  $\alpha$ –nickel hydroxide by coating with  $\beta$ –nickel hydroxide, *Journal of Power Sources*, 224 (2013) 236–240.
- [48] M. Hu, Z. Yang, L. Lei, Y. Sun, Structural transformation and its effects on the electrochemical performances of a layered double hydroxide, *Journal of Power Sources*, 196 (2011) 1569–1577.
- [49] K. Suresh, M. Kumar, G. Pugazhenthii, R. Uppaluri, Enhanced mechanical and thermal properties of polystyrene nanocomposites prepared using organo–functionalized Ni–Al layered double hydroxide via melt intercalation technique, *Journal of Science Advanced Materials & Devices*, 2 (2017) 245–254.
- [50] J. Shi, L. Lai, P. Zhang, H. Li, Y. Qin, Y. Gao, L. Luo, J. Lu, Aluminum doped nickel oxide thin film with improved electrochromic performance from layered double hydroxides precursor in situ pyrolytic route, *Journal of Solid State*

Chemistry, 241 (2016) 1–8.

- [51] Z. Sun, C. Lin, J. Zheng, L. Wang, J. Zhang, F. Xu, J. Hou, Fabrication and characterization of hierarchical Mg/Ni/Al layered double hydroxide framework on aluminum foam, *Materials Letter*, 113 (2016) 83–86.

ACCEPTED MANUSCRIPT

## Figure Captions

Fig.1 Schematic diagram of the formation mechanism of the nano Ni/Al LDHs

(1, Nucleation process; 2, Growth process; 3, Migration process)

Fig. 2 SEM and EDX mapping images of the Ni/Al LDHs samples with different Al contents (a, pure Ni(OH)<sub>2</sub>; b, 3% Al; c, 6% Al; d, 9% Al; e, 12% Al; f, 15% Al; g, 18% Al; h, 21% Al) and their corresponding XRD patterns (\*,  $\alpha$ -Ni(OH)<sub>2</sub>; ●,  $\beta$ -Ni(OH)<sub>2</sub>).

Fig. 3 a, CV curves of different Al-doped samples at a scan rate of 10 mV s<sup>-1</sup>; b, specific charge and discharge capacities of the above samples during the CV tests by integral method; c, galvanostatic charge–discharge curves of LDHs electrodes containing various Al contents at a current density of 2 A g<sup>-1</sup>; d, specific capacity of the LDHs electrodes containing various Al contents at different current densities.

Fig. 4 Status of the Ni/Al LDHs samples with different Al contents (a, 0% Al; b, intermediate Al contents; c, extra high Al contents); d, interplanar spacing *c* of Ni/Al LDHs samples with different Al contents; e, exchange current density of Ni/Al LDHs samples with different Al contents.

Fig. 5 a, XRD patterns of the Ni/Al LDHs (18% Al) electrode during charge and discharge processes (★, Ni/Al LDHs; ●,  $\gamma$ -NiOOH; ◆, Ni); b, XPS spectra of Ni element in the Ni/Al LDHs (18% Al) electrode during charge and discharge processes; c and e, TEM images of Ni/Al LDHs (18% Al) electrode before charge and discharge, respectively; d and f, Ni/Al LDHs (18% Al) after 5000 cycles.

Fig. 6 a, CV curves of Ni/Al LDHs (18% Al) electrode a scan rate of 50 mV s<sup>-1</sup>; b, specific charge and discharge capacity of the Ni/Al LDHs (18% Al) electrode during

the CV tests by integral method; c, cycling life curves of Ni/Al LDHs (18% Al) at different charge discharge rates; d, comparison of the specific capacity of the LDHs electrodes and the relevant Ni based cathode materials in the literature.

ACCEPTED MANUSCRIPT

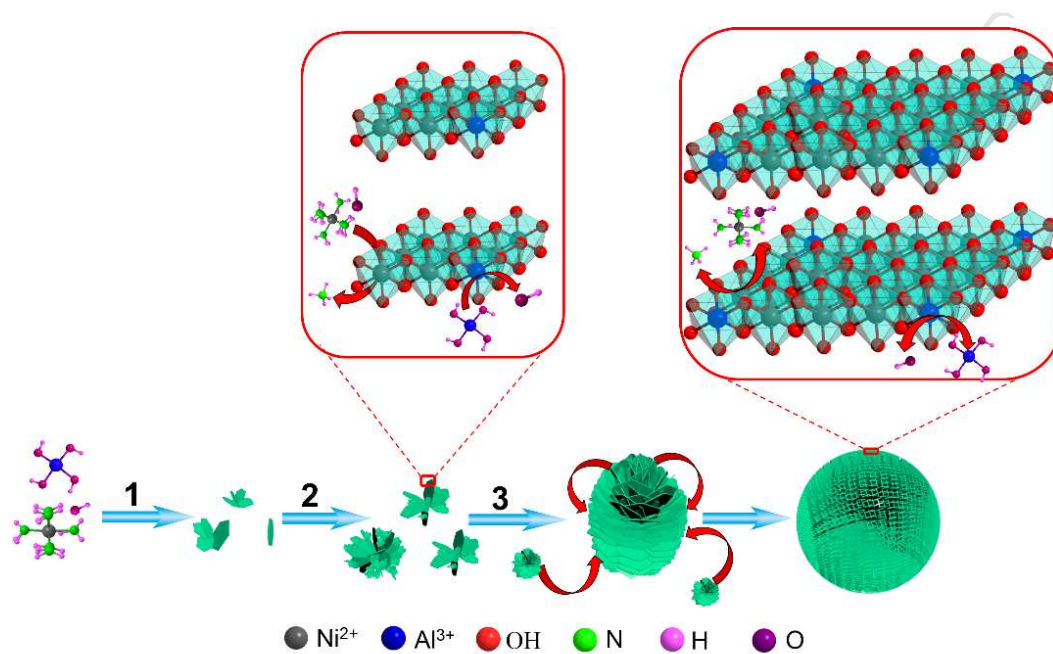


Fig. 1

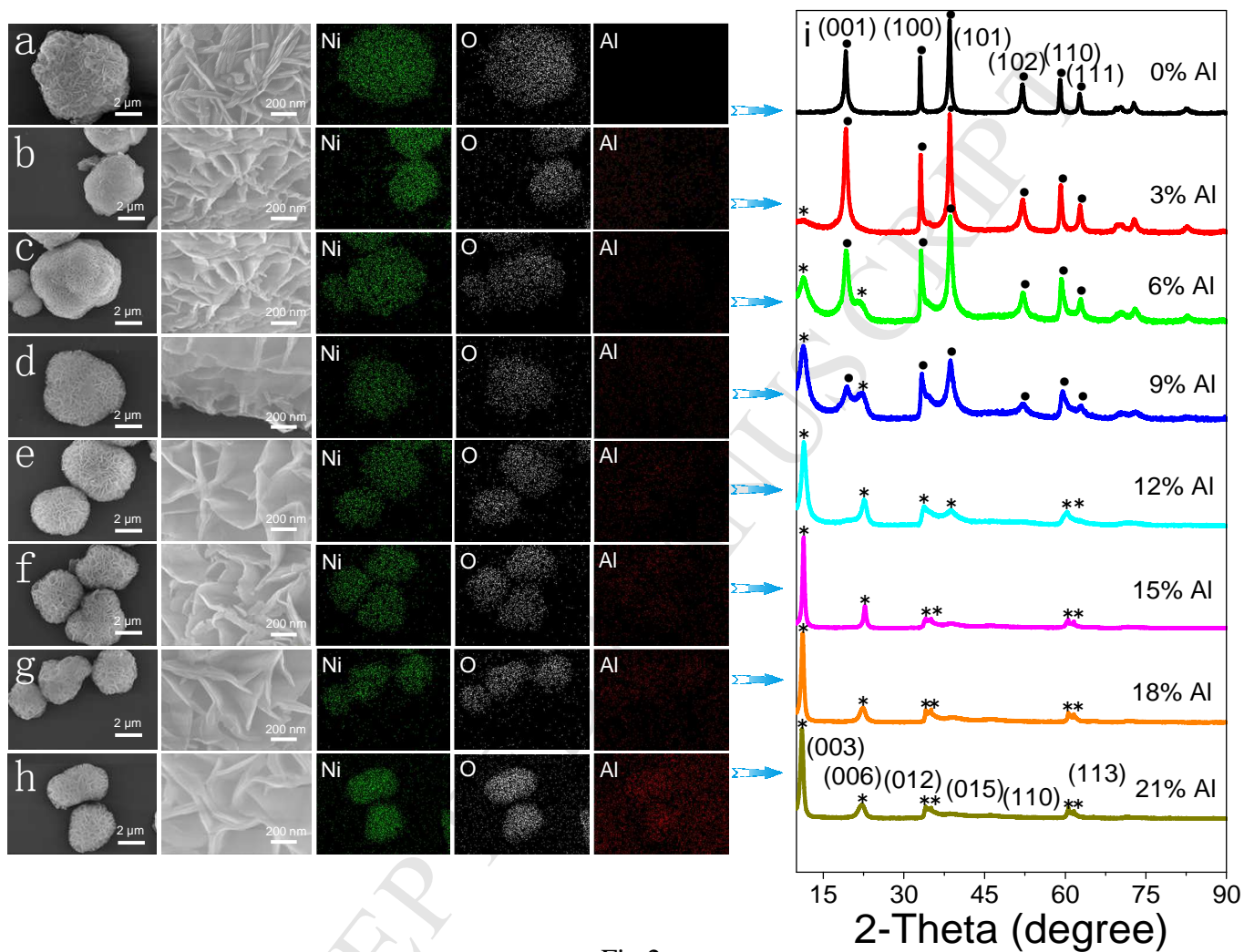


Fig.2

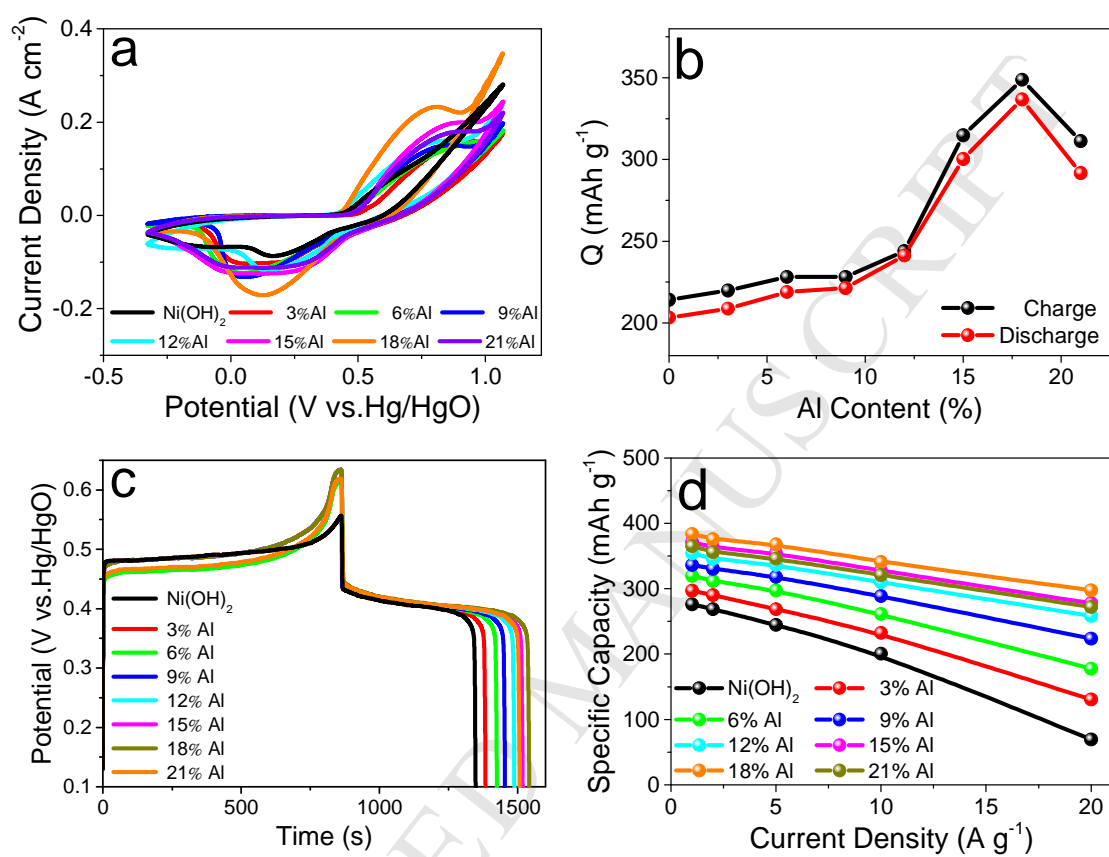


Fig.3

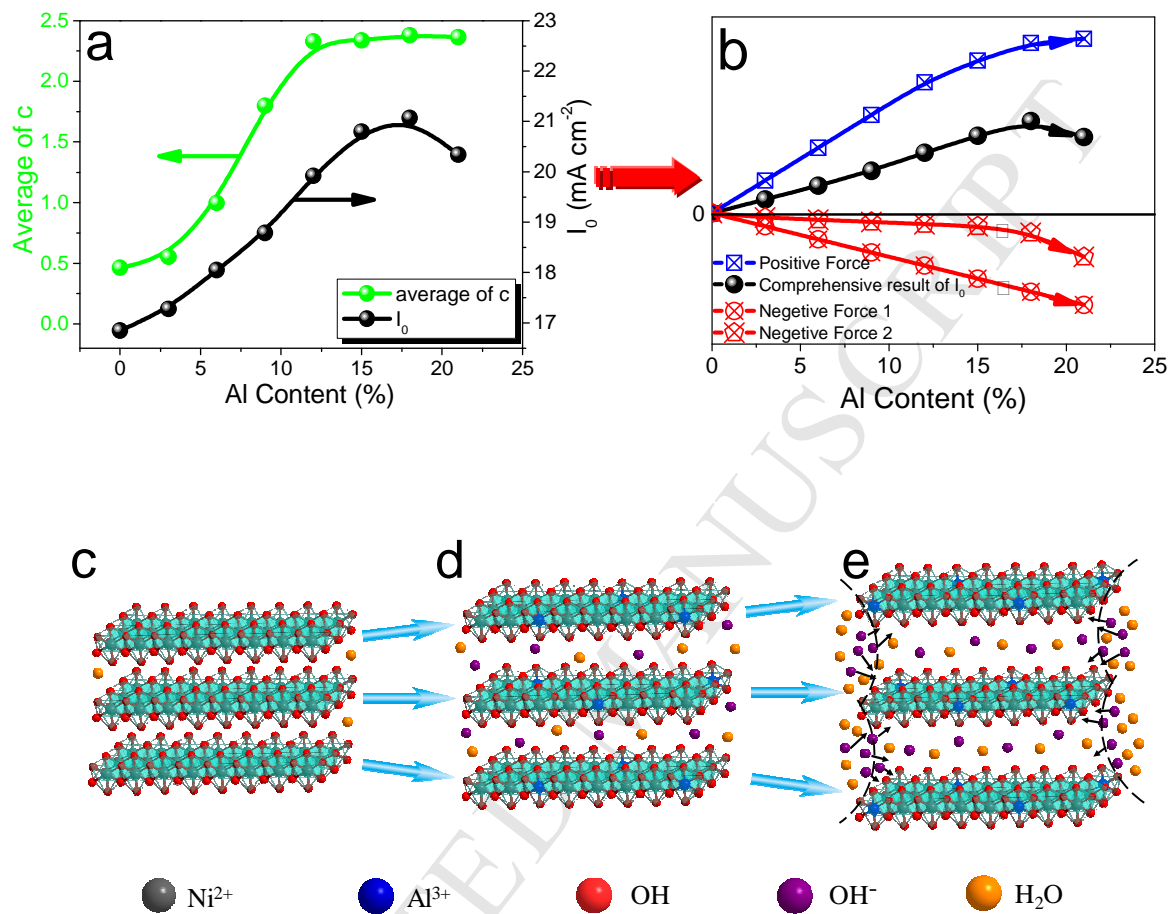


Fig.4

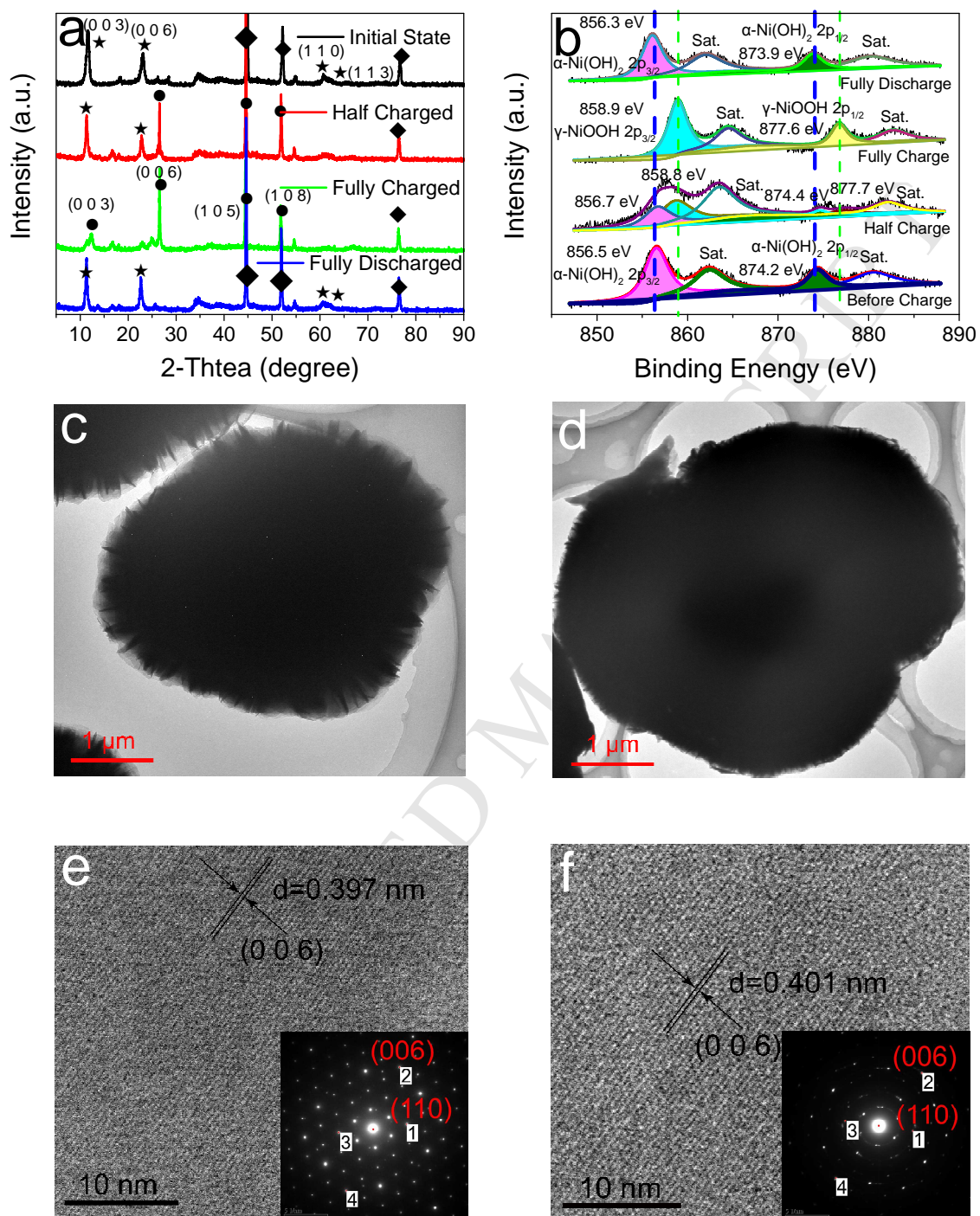


Fig. 5

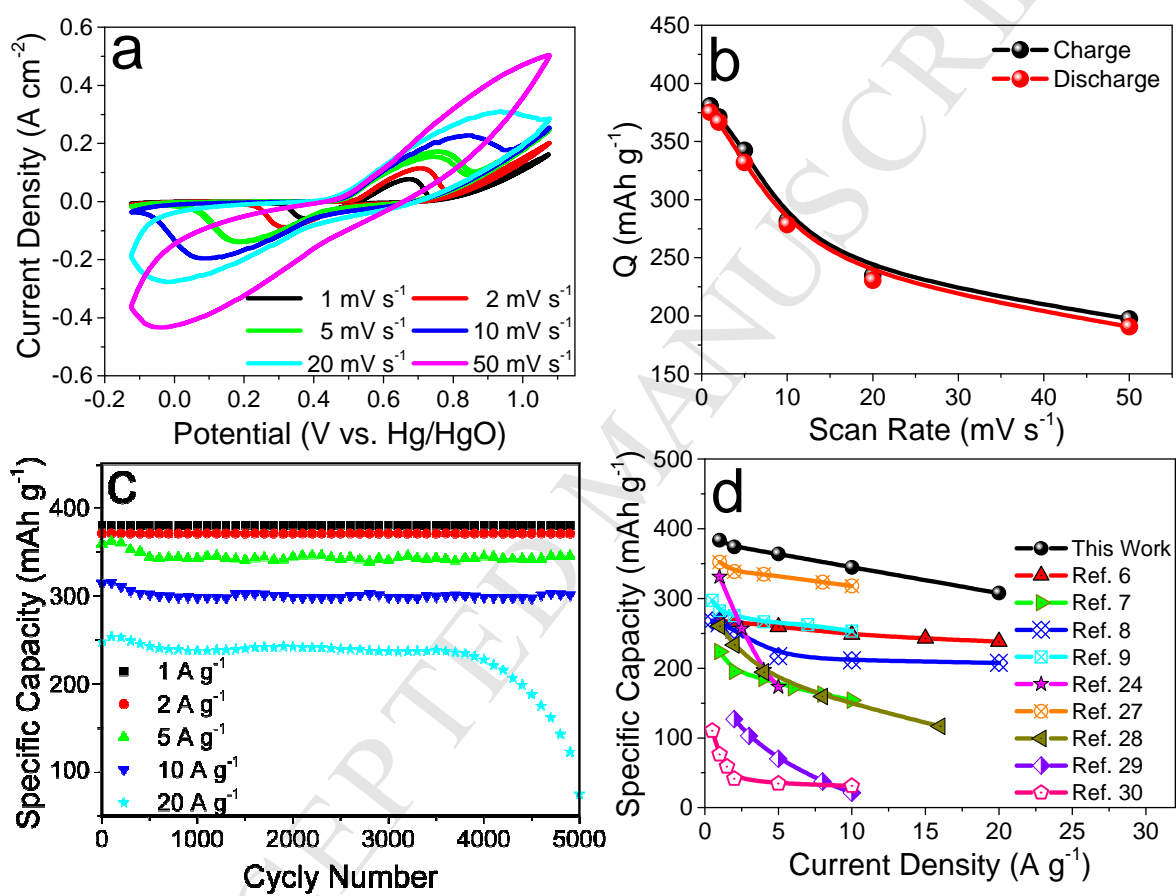


Fig.6

**Highlights**

- Spherical Ni/Al LDHs with nanostructure is synthesized by a stable DCP method.
- The doping of Al<sup>3+</sup> effectively controls the distance of LDHs layer and its interior forces.
- The optimal doping of Al<sup>3+</sup> shows superior properties to other reported Ni/Al LDHs.
- The obtained Ni/Al LDHs with 18% Al provides the maximum capacity of 383.4 mAh g<sup>-1</sup> at 1 A g<sup>-1</sup>.

## Supporting Information

### **Preparation of 3D spherical Ni/Al LDHs with significantly enhanced electrochemical performance as a superior cathode material for Ni/MH batteries**

Yajing Nie<sup>a</sup>, Wei Li<sup>b</sup>, Junqing Pan<sup>a\*</sup>, Raja A. Senthil<sup>a</sup>, Carlos Fernandez<sup>d</sup>, Yanzhi Sun<sup>c</sup>, Jianjun

Liu<sup>a</sup>

*<sup>a</sup> State Key Laboratory of Chemical Resource Engineering, Beijing University of Chemical Technology, Beijing 100029, China*

*<sup>b</sup> Department of Engineering Technology and Texas Center for Superconductivity, University of Houston, Houston, TX 77204, USA*

*<sup>c</sup> National Fundamental Research Laboratory of New Hazardous Chemicals Assessment and Accident Analysis, Beijing University of Chemical Technology, Beijing 100029, China.*

*<sup>d</sup> School of Pharmacy and Life Sciences, Robert Gordon University, Aberdeen, AB10 7GJ, UK*

\* Corresponding authors:

Tel./Fax: +86-10-64448461

E-mails: [jqpan@mail.buct.edu.cn](mailto:jqpan@mail.buct.edu.cn) (J. Pan)

### **Figure caption**

Fig. S1 a, Nyquist plots of the Ni/Al LDHs electrodes with different Al contents; b, polarization curves of the Ni/Al LDHs electrodes with different Al contents.

(EIS frequency range: 0.1–10<sup>5</sup>Hz; scan range of Tafel tests: 0.3–0.7 Vs Hg/HgO Ref. electrode; Electrolyte: 1.0 mol L<sup>-1</sup> KOH)

### **Table captions**

Table S1 BET surface areas of the Ni/Al LDHs samples with different Al contents.

Table S2 Interplanar spacing values of Ni/Al LDHs samples with different Al contents.

Table S3 Exchange current densities of Ni/Al LDHs samples with different Al contents.

Table S4 Specific capacities of charge and discharge for the Ni/Al LDHs electrodes with different Al contents during the CV tests by integral method.

Table S5 Specific charge and discharge capacities of Ni/Al LDHs electrodes during the CV tests by integral method at different scan rates.

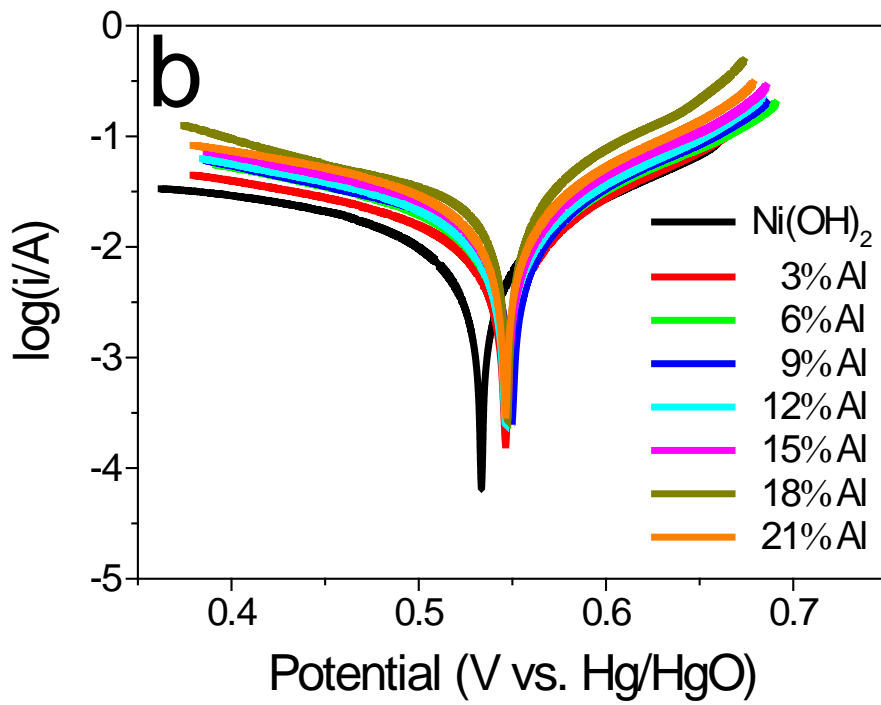
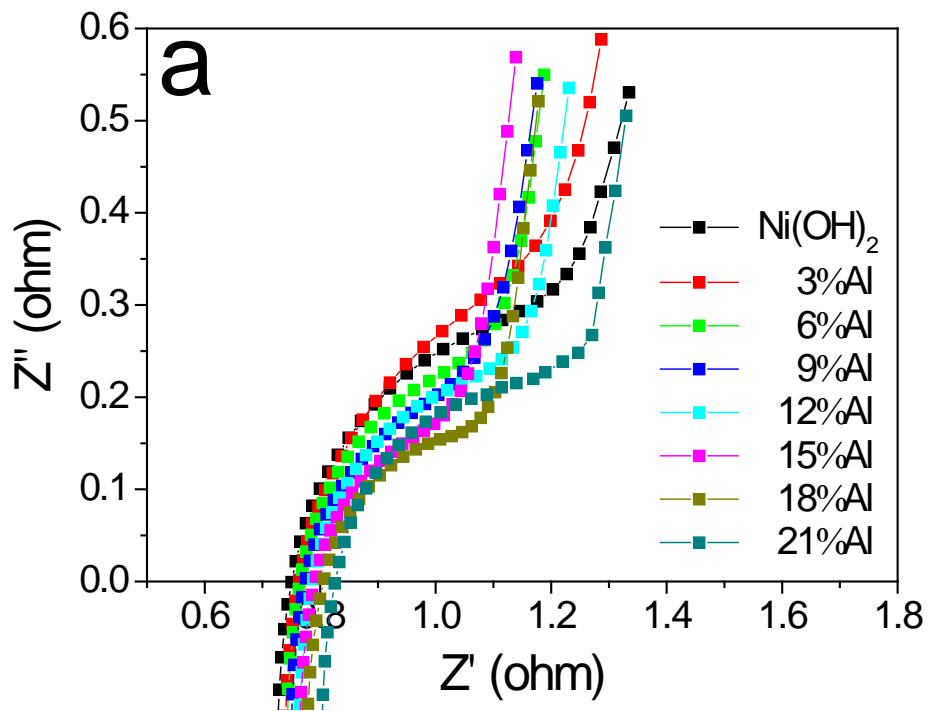


Fig. S1

Table S1

Al content (%)	BET Surface Area (m <sup>2</sup> /g)
Ni(OH) <sub>2</sub>	9.7
3	14.0
6	18.2
9	22.6
12	27.4
15	32.1
18	36.3
21	31.3

Table S2

Al content (%)	crystal form	hkl	2 $\theta$ (°)	d (nm)	FWH (°)	D (nm)	a (nm)	$\bar{a}$ (nm)	c (nm)	$\bar{c}$ (nm)
0	100% $\beta$	001	19.124	0.4639	0.549	14.5057				
		100	33.272	0.2707	0.303	27.0496	0.3126	0.3126	0.4639	0.4639
		101	38.422	0.2340	0.476	17.4707				
3	95% $\beta$	001	19.230	0.4612	0.641	12.4257				
		100	33.112	0.2703	0.342	23.9550	0.3121	0.3121	0.4612	0.5530
		101	38.518	0.2335	0.557	14.9344				
	5% $\alpha$	003	11.54	0.7662	0.38	20.7709	---		2.2985	
6	71% $\beta$	001	19.332	0.4588	0.733	10.8677				
		100	33.194	0.2697	0.391	20.9574	0.3114	0.3114	0.4588	0.9976
		101	38.62	0.2329	0.632	13.1663				
	29% $\alpha$	003	11.449	0.7722	0.839	9.4068	---		2.3167	
9	28% $\beta$	001	19.455	0.4559	0.661	12.0537				
		100	33.337	0.2686	0.455	18.0163	0.3101	0.3103	0.4559	1.7982
		101	38.66	0.2327	0.751	11.0814				
	72% $\alpha$	003	11.286	0.7734	0.87	9.0703				
		006	22.485	0.3951	0.848	9.4417	0.3104		2.3202	
		110	59.505	0.1552	0.682	13.2630				
12	100% $\alpha$	003	11.388	0.7764	0.737	10.7081				
		006	22.669	0.3919	0.777	10.3078	0.3088	0.3088	2.3291	2.3291
		110	59.855	0.1544	0.695	13.0377				
15	100% $\alpha$	003	11.347	0.7792	0.441	12.3114				
		006	22.732	0.3908	0.813	9.8507	0.3065	0.3065	2.3374	2.3374
		110	60.344	0.1533	0.464	19.5767				
18	100% $\alpha$	003	11.143	0.7934	0.556	14.1911				
		006	22.383	0.3969	0.834	9.5986	0.3053	0.3053	2.3801	2.3801
		110	60.61	0.1526	0.429	21.2026				
21	100% $\alpha$	003	11.06	0.7883	0.592	13.3272				
		006	22.239	0.3994	0.883	9.0636	0.3057	0.3057	2.3649	2.3649
		110	60.529	0.1528	0.488	18.6314				

Table S2 presents the lattice parameters calculated from the XRD spectra of Figure 2 by Scherrer formula, and the Scherrer formula is as follows:

$$D = \frac{K\lambda}{B \cos\theta}$$

Where “K” is Scherrer constant,  $K = 0.89$ , “B” is half width is full width of half maximum (FWHM),  $\theta$  is diffraction angle,  $\lambda$  is the X-ray wavelength,  $\lambda = 0.154$  nm.

Because the Ni/Al LDHs belong to hexagonal crystal system, its unit lattice parameters have the relationship of  $a = b \neq c$ ,  $\alpha = \beta = 90^\circ$  and  $\gamma = 120^\circ$ , and its lattice parameter calculation formula can be simplified as:

$$\frac{1}{d_{hkl}^2} = \frac{4(h^2 + hk + k^2)}{3a^2} + \frac{l^2}{c^2}$$

Using the formula, the a, b and c can be calculated.

Table S3

Al content (%)	$k_a$	$k_c$	$I_0$ ( $A\text{ cm}^{-2}$ )	$E_0$ (V vs. Hg/HgO)
Ni(OH) <sub>2</sub>	10.014	4.292	0.01685	0.531
3	7.814	3.911	0.01748	0.537
6	8.367	4.532	0.01805	0.536
9	8.201	4.650	0.01862	0.538
12	7.764	4.637	0.01962	0.538
15	7.232	4.011	0.02040	0.537
18	7.646	3.904	0.02107	0.538
21	7.673	4.596	0.02004	0.537

Table S4

Al Content (%)	Charge Capacity (mAh g <sup>-1</sup> )	Discharge Capacity (mAh g <sup>-1</sup> )
0	214.2	203.3
3	219.9	208.8
6	228.2	218.9
9	228.1	221.4
12	243.9	241.3
15	314.8	300.3
18	348.8	336.7
21	311.2	291.7

Table S5

Scan Rate (mV s <sup>-1</sup> )	Charge Capacity (mAh g <sup>-1</sup> )	Discharge Capacity (mAh g <sup>-1</sup> )
1	380.6	375.2
2	371.3	366.9
5	342.4	332.0
10	281.9	278.6
20	234.9	230.6
50	197.4	190.7